Equilibration of the Gluon-Minijet Plasma at RHIC and LHC

Gouranga C. Nayak[a], Adrian Dumitru[b], Larry McLerran[c], Walter Greiner[a]
[a] *Institut für Theoretische Physik, J. W. Goethe-Universität, 60054 Frankfurt am Main, Germany*
[b] *Department of Physics, Columbia University, 538W 120th Street, New York, NY 10027, USA*
[c] *Physics Department, Brookhaven National Laboratory Upton, NY 11979, USA*

Abstract

We study the production and equilibration of the gluon-minijet plasma expected to be formed in the central region of ultrarelativistic heavy-ion collisions at the BNL-RHIC and the CERN-LHC by solving a self-consistent relativistic transport equation. We compute the minijet production within perturbative QCD. Subsequent collisions among the semi-hard partons are treated by considering the elastic $gg \to gg$ processes with screening of the long wavelength modes taken into account. We determine the time τ_{eq} where close to ideal hydrodynamic flow sets in, and find rather similar numbers for central heavy-ion collisions at BNL-RHIC and CERN-LHC energies. The number densities, energy densities and temperatures of the minijet plasma are found to be different at RHIC and LHC, e.g. $T(\tau_{eq}) \sim 220$ MeV and 380 MeV, respectively.

PACS: 12.38.Mh, 25.75.-q, 13.87.-a, 24.85.+p

I. INTRODUCTION

In the next few years, the BNL-RHIC (Au-Au collisions at $\sqrt{s}$=200 GeV per incident nucleon pair) and the CERN-LHC (Pb-Pb collisions at $\sqrt{s}$=5.5A TeV) accelerators will provide the opportunity to study a new phase of matter, namely the so-called Quark-Gluon Plasma (QGP) [1]. It is very important and interesting to study whether the QGP actually does thermalize in those reactions, and if so, what is the actual energy density, number density and temperature at which it thermalized. For this purpose, and also for the calculation of all the signatures, it is necessary to study the space-time evolution of partons just after the nuclear collision. For example, the equilibration time is crucial for a quantitative understanding of J/ψ suppression [2], and it is a challenging task to determine this quantity accurately. Similarly, understanding the equilibration time is important for all other proposed signatures for the QGP, for example for dilepton emission and strangeness production [1]. Once equilibrium is reached, the further space time evolution of partons can be described by the well known equations of hydrodynamics.

The evolution of the QGP towards (local) equilibrium can be studied by solving transport equations for quarks and gluons with all the dynamical effects taken into account. Obviously, the first problem one always encounters is the correct computation of the initial conditions needed to solve the transport equation. This is because one can not calculate the parton production in all range of momentum from perturbative QCD (pQCD). There are also coherence effects [3,4] that play an important role in the early stage of the nuclear collision at very high energy. For small x and large nuclei, the QCD based calculation performed in [5] predicts the existence of a coherent field in a certain kinematical range. That field may play an important role in the equilibration of the plasma. In the present paper, however, we restrict our calculation to the initial incoherent parton production, which is computed within the framework of pQCD. We study the subsequent evolution of that minijet "plasma" by solving a relativistic transport equation, thus taking into account collisions between the produced partons. In the future, we intend to generalize our approach to include both coherent field and incoherent partons in the transport equation.

The paper is organized as follows. In section II we briefly review minijet production in high-energy nuclear collisions within pQCD. In section III we discuss the in-medium screening of long wavelength gluons which is relevant to our study. We present the relativistic transport equation in section IV, briefly describing the numerical strategy for its solution in section V. We discuss our main results in section VI and conclude in section VII. Throughout the manuscript we employ natural units, $\hbar = c = k = 1$.

II. MINIJET PRODUCTION IN NUCLEAR COLLISIONS AT RHIC AND LHC

In this section we review the computation of the single-inclusive semi-hard cross section in lowest order pQCD, cf. also [6,7]. The $2 \rightarrow 2$ minijet cross section per nucleon in AA collision is given by

$$\sigma_{jet} = \int dp_t dy_1 dy_2 \frac{2\pi p_t}{\hat{s}} \sum_{ijkl} x_1 \ f_{i/A}(x_1, p_t^2) \ x_2 \ f_{j/A}(x_2, p_t^2) \ \hat{\sigma}_{ij\rightarrow kl}(\hat{s}, \hat{t}, \hat{u}). \tag{1}$$

Here x_1 and x_2 are the light-cone momentum fractions carried by the partons i and j from the projectile and the target, respectively. $f_{j/A}$ are the distribution functions of the parton species j within a nucleon bound in a nucleus of mass number A. y_1 and y_2 denote the rapidities of the scattered partons. The symbols with carets refer to the parton-parton c.m. system. $\hat{\sigma}_{ij\to kl}$ is the elementary pQCD parton cross section.

$$\hat{s} = x_1 x_2 s = 4p_t^2 \cosh^2\left(\frac{y_1 - y_2}{2}\right), \tag{2}$$

gives the total c.m.-energy of the parton-parton scattering. The rapidities y_1, y_2 and the momentum fractions x_1, x_2 are related by,

$$x_1 = p_t\ (e^{y_1} + e^{y_2})/\sqrt{s}, \qquad x_2 = p_t\ (e^{-y_1} + e^{-y_2})/\sqrt{s}. \tag{3}$$

The limits of integrations of rapidities y_1 and y_2 are given by $|y_1| \leq \ln(\sqrt{s}/2p_t + \sqrt{s/4p_t^2 - 1})$ and $-\ln(\sqrt{s}/p_t - e^{-y_1}) \leq y_2 \leq \ln(\sqrt{s}/p_t - e^{y_1})$, respectively. We multiply the above minijet cross sections by the phenomenological factor $K = 2$ to account for higher-order contributions.

The minijet cross section, Eq. (1), can be related to the total number of produced partons via

$$N = T(0) \int dp_t dy_1 dy_2 \frac{2\pi p_t}{\hat{s}} \sum_{ijkl} x_1\ f_{i/A}(x_1, p_t^2)\ x_2\ f_{j/A}(x_2, p_t^2)\ \hat{\sigma}_{ij\to kl}(\hat{s}, \hat{t}, \hat{u}), \tag{4}$$

where $T(0) = 9A^2/8\pi R_A^2$ is the nuclear geometrical factor for head-on AA collisions (for a nucleus with a sharp surface). $R_A = 1.1A^{1/3}$ fm is the nuclear radius. Similarly, the total transverse energy E of minijets is given by

$$E = T(0) \int dp_t p_t dy_1 dy_2 \frac{2\pi p_t}{\hat{s}} \sum_{ijkl} x_1\ f_{i/A}(x_1, p_t^2)\ x_2\ f_{j/A}(x_2, p_t^2)\ \hat{\sigma}_{ij\to kl}(\hat{s}, \hat{t}, \hat{u}). \tag{5}$$

We employ the "EKS98" set of parton distribution functions in a bound nucleon from ref. [8], based on the GRV98 set of parton distributions for a free nucleon [9]. One has to choose the scale in the transverse momentum below which the incoherent parton picture is not valid and coherence effects have to be taken into account. These scales provide the initial cutoff for the (semi-)hard scatterings. The values for the cutoff are found to be ~ 1 at RHIC and ~ 2 GeV at LHC from the McLerran-Venugopalan model using their initial conditions [4]. For the quantitative estimates presented below we actually choose the cutoff p_0 to be 1.13 GeV and 2.13 GeV at RHIC and LHC, respectively. These values are obtained by an independent method by Eskola *et. al,* [10].

To solve the transport equation one has to specify the initial distribution function of the particles in phase-space, while accounting for the correlation between momentum-space rapidity and space-time rapidity. We choose our initial distribution function to be a Boltzmann distribution in the local rest frame,

$$f(\tau_0 = 1/p_0, \xi, p_t) = \exp\left(-p_\mu u^\mu / T_{jet}\right) = \exp\left(-p_t \cosh\xi / T_{jet}\right). \tag{6}$$

$u^\mu = (\cosh\eta, 0, 0, \sinh\eta)$ is the four-velocity of the local rest-frame of the medium, with $\eta = \mathrm{Artanh}\,(z/t)$ denoting the space-time rapidity, and $\xi \equiv \eta - y$. The parameter T_{jet} can

be determined from the average energy per particle of the initially formed minijets which is obtained from Eqs. (5) and (4). We mention here that even though the initial distribution is chosen to be a Boltzmann distribution, the subsequent evolution will be non-ideal, see below.

We shall use these initial conditions to study the evolution of the parton "plasma" at RHIC and LHC by solving a self-consistent relativistic transport equation (see section IV). As most of the produced minijets are gluons, we will simplify our considerations by considering gluons only. In Table-I we have listed the initial conditions of the gluon minijets.

III. SCREENING IN NON-EQUILIBRIUM

In this section we describe the screening of long wavelength electric fields in the parton medium. It will play an important role in defining the finite collision term of our transport equation. We shall employ the static limit (screening of infinitely long wavelength fields), which gives the Debye screening mass, and assume that this simplified treatment is at least qualitatively correct. Our concern here is to incorporate the density dependence of the medium-induced cutoff (which thus also depends on collision energy), as well as to treat the coupled evolution (cutoff and medium) self-consistently. At present we can not include magnetic (dynamic) screening into the non-equilibrium study because we do not find an expression for the magnetic screening mass in terms of the non-equilibrium distribution function in the literature (see section VII for a detail discussion). We also mention here that the momentum dependent screening mass is usually studied in thermal equilibrium. However, accounting for the momentum dependence of the screening mass in non-equilibrium is technically very difficult and is beyond the scope of this present paper.

The electric screening mass is given by the infrared limit of the real part of the gluon self-energy Π^{00}, calculated in the given background that is described by the distribution function f (not to be confused with the parton distribution function $f_{j/A}$ introduced in section II). In ref. [11] the following expression has been derived (in Coulomb gauge) for a medium of gluonic excitations:

$$m^2 = -\frac{3\alpha_s}{\pi^2} \lim_{|\vec{q}|\to 0} \int d^3p \, \frac{|\vec{p}|}{\vec{q}\cdot\vec{p}} \vec{q}\cdot\nabla_p f(p). \tag{7}$$

In the above equation $\vec{q}$ is the momentum of the test particle, $f(p)$ is the non-equilibrium distribution function of the gluons and α_s is the strong coupling constant. We will consider the transverse screening mass in the following, which will be introduced below as a cutoff in parton-parton anti-collinear elastic scattering to obtain a finite transport cross-section. Performing an integration by parts we obtain the transverse screening mass

$$m_t^2 = \frac{3\alpha_s}{\pi^2} \int \frac{\mathrm{d}^3p}{p^0} f(p). \tag{8}$$

Following Bjorken's hypothesis [12], we express all quantities in terms of longitudinal-boost invariant parameters $\tau = \sqrt{t^2 - z^2}$, ξ and p_t. We assume that the above equation is also valid for a space-time dependent distribution function $f(x,p)$ and hence use

$$m_t^2(\tau) = \frac{6\alpha_s(\tau)}{\pi} \int dp_t p_t \int d\xi \, f(\tau, p_t, \xi) \quad . \tag{9}$$

Improving earlier approaches [13], we do not assume factorization of the distribution function in the form $f(\tau, p_t, \xi) = g(\xi)h(\tau, p_t)$. Also, in our case the screening mass enters the collision kernel of the transport equation and thus determines the rate of equilibration.

In the above equation the QCD running coupling constant becomes time dependent, via

$$\alpha_s(\tau) = \alpha_s(\langle p_t^2(\tau)\rangle). \tag{10}$$

The average transverse momentum squared of the excitations of the medium is defined as

$$\langle p_t^2(\tau)\rangle = \frac{\int d\Gamma p_\mu u^\mu p_t^2 f(\tau, p_t, \xi)}{\int d\Gamma p_\mu u^\mu f(\tau, p_t, \xi)}. \tag{11}$$

Here $\mathrm{d}\Gamma = \mathrm{d}^3p/(2\pi)^3 p^0 = \mathrm{d}p_t p_t \mathrm{d}\xi/(2\pi)^2$ is the invariant momentum-space measure. Throughout the manuscript we use the GRV98 calculation of $\alpha_s(\langle p_t^2(\tau)\rangle)$ [9] with $\langle p_t^2(\tau)\rangle$ calculated from Eq. (11).

IV. SOLUTION OF THE TRANSPORT EQUATION WITH SCREENING

In the absence of any coherent color field the space-time evolution of the produced partons at RHIC and LHC can be studied by solving the Boltzmann transport equation

$$p^\mu \partial_\mu f(x, p) = C(x, p), \tag{12}$$

where $f(x, p)$ is the distribution function of gluons and $C(x, p)$ is the collision term. To solve the above transport equation with the initial value of f_0 given by Eq. (6), we employ the relaxation time approximation for the collision term [14,15]:

$$C(\tau, \xi, p_t) = -p^\mu u_\mu \left[f(\tau, \xi, p_t) - f^{eq}(\tau, \xi, p_t)\right]/\tau_c(\tau). \tag{13}$$

f^{eq} is the Bose-Einstein equilibrium distribution function, and $\tau_c(\tau)$ is the time dependent relaxation time of the plasma. With this collision term the formal solution of the transport equation becomes

$$f(\tau, \xi, p_t) = \int_{\tau_0}^{\tau} \mathrm{d}\tau' \exp\left(\int_{\tau}^{\tau'} \frac{\mathrm{d}\tau''}{\tau_c(\tau'')}\right) \frac{f^{eq}(\tau', \xi', p_t)}{\tau_c(\tau')} + \; f(\tau_0, \xi_0, p_t) \; \exp\left(-\int_{\tau_0}^{\tau} \frac{\mathrm{d}\tau''}{\tau_c(\tau'')}\right), \tag{14}$$

where ξ' is the solution of

$$\sinh\xi' = \frac{\tau}{\tau'}\sinh\xi \;, \tag{15}$$

and $\sinh\xi_0 = \frac{\tau}{\tau_0}\sinh\xi$, with $\tau_0 = 1/p_0$. Despite the fact that the transport cross section (governing kinetic equilibration) has been derived from the $gg \to gg$ elastic scattering cross section, the number-current of the gluons is not conserved. Rather, for massless particles the number density in equilibrium is proportional to the entropy density. However, dissipation during the pre-equilibrium stage will produce additional entropy, and accordingly the comoving number density is expected to decrease less fast than for a conserved current $j^\mu = \rho u^\mu$, where $\partial_\mu(\rho u^\mu) = \mathrm{d}\rho/\mathrm{d}\tau + \rho/\tau = 0$, see below.

We write the relaxation time for collisions, $\tau_c(\tau)$, as

$$\tau_c(\tau) = \frac{1}{\sigma_t(\tau) n(\tau)} \quad , \tag{16}$$

where

$$n(\tau) = g_G \int \mathrm{d}\Gamma p_\mu u^\mu f(\tau, p_t, \xi) \tag{17}$$

is the number density of the gluon-minijet plasma, and

$$\sigma_t(\tau) = \int \mathrm{d}\Omega \frac{\mathrm{d}\sigma}{\mathrm{d}\Omega} \sin^2\theta_{c.m.} \tag{18}$$

denotes the time dependent transport cross-section for the collision processes [15,16]. We assume that anti-collinear small-angle scattering gives the dominant contribution to the transport cross-section [16], such that $\sin^2\theta_{c.m.} = 4\hat{t}\hat{u}/\hat{s}^2$. We mention again that, in our study, all the quantities such as m_t, σ_t, n, τ_c are time dependent and have been obtained from the non-equilibrium distribution function of the gluon minijets.

We shall consider the leading order elastic scattering processes $gg \rightarrow gg$. The differential cross section for this process is given by

$$\frac{\mathrm{d}\sigma}{\mathrm{d}\hat{t}} = \frac{9\pi\alpha_s^2}{2\hat{s}^2}\left[3 - \frac{\hat{u}\hat{t}}{\hat{s}^2} - \frac{\hat{u}\hat{s}}{\hat{t}^2} - \frac{\hat{s}\hat{t}}{\hat{u}^2}\right]. \tag{19}$$

In the limit of small-angle scattering (of identical particles) it simplifies to

$$\frac{\mathrm{d}\sigma}{\mathrm{d}\hat{t}} = \frac{9\pi\alpha_s^2}{2}\frac{1}{\hat{t}^2} \tag{20}$$

and the transport cross-section σ_t diverges logarithmically due to exchange of long-wavelength gluons. However, as discussed in section III, long-wavelength fields will be screened by the dense medium. For our studies we therefore employ the medium-modified elastic cross-section [17]

$$\frac{\mathrm{d}\sigma}{\mathrm{d}\hat{t}} = \frac{9\pi\alpha_s^2}{2}\left(\frac{m_t^2}{\hat{s}} + 1\right)\frac{1}{\left(\hat{t} - m_t^2\right)^2} \quad . \tag{21}$$

Using Eq. (21) in Eq. (18) we obtain the medium modified finite (time dependent) transport cross-section

$$\sigma_t(\tau) = \frac{9}{2}\frac{4\pi\alpha_s^2(\tau)}{\hat{s}^2(\tau)}\left(\frac{m_t^2(\tau)}{\hat{s}(\tau)} + 1\right)\left[\left(\hat{s}(\tau) + 2m_t^2(\tau)\right)\log\left(\frac{\hat{s}(\tau)}{m_t^2(\tau)} + 1\right) - 2\hat{s}(\tau)\right] \quad . \tag{22}$$

To simplify the considerations we have replaced $\hat{s}$ by its average value

$$\hat{s}(\tau) = 4\langle E(\tau)\rangle^2 \tag{23}$$

in the above expression. $\langle E(\tau)\rangle$ is the time dependent average energy per particle given by

$$\langle E(\tau)\rangle = \frac{\epsilon(\tau)}{n(\tau)}, \tag{24}$$

where

$$\epsilon(\tau) = g_G \int \mathrm{d}\Gamma (p_\mu u^\mu)^2 f(\tau, p_t, \xi) \tag{25}$$

is the energy density of the minijet "plasma" and $n(\tau)$ is the local number density as defined in Eq. (17).

To obtain the collision term (13) in each time step we also have to determine the equilibrium distribution towards which the evolution is supposed to converge. In other words, we have to determine the "equivalent" plasma temperature from (25). It can be obtained from the condition that the first moment of the actual distribution function f equals that of the equilibrium distribution function f^{eq}, i.e.

$$\epsilon = g_G \frac{\pi^2}{30} T^4. \tag{26}$$

This should be a reasonable approximation as long as the system is not very close to the hadronization phase transition.

V. NUMERICAL SOLUTION

The expression for the distribution function $f(\tau, \xi, p_t)$, Eq. (14), involves $T(\tau)$ and $\tau_c(\tau)$ which are again defined through the distribution function $f(\tau, \xi, p_t)$. We solve these coupled set of equations self-consistently. At any time τ we start with the old trial values T_O, n_O, α_{sO}, m_{tO} and $\hat{s}_O$ from which we get f_O via Eq. (14). This f_O is used in Eq. (25) to calculate $\epsilon(\tau)$ which gives a new temperature T_N through Eq. (26). This new temperature, but the old values of n_O, α_{sO}, m_{tO} and $\hat{s}_O$ are again used in Eq. (14) to get a new f_1. This f_1 is used in Eq. (17) to calculate a new n_N which also gives a new value $\hat{s}_N$ via Eq. (23). These new values T_N, n_N and $\hat{s}_N$ and the old values α_{sO} and m_{tO} are again used in Eq. (14) to get a new f_2. Using this f_2 in Eq. (11) we obtain α_{sN} from Eq. (10). These new values T_N, n_N, $\hat{s}_N$, α_{sN} and old value m_{tO} are again used in Eq. (14) to obtain a new f_3. Using this f_3 in Eq. (9) we obtain a new m_{tN}. Thus, starting with the old set of values T_O, n_O, α_{sO}, m_{tO} and $\hat{s}_O$ we obtain a new set of values T_N, n_N, α_{sN}, m_{tN} and $\hat{s}_N$. This process is iterated until convergence is attained to the required accuracy. This gives us the self-consistent values of $\epsilon(\tau)$, $T(\tau)$, $n(\tau)$, $\alpha_s(\tau)$, $m_t(\tau)$ and $\hat{s}(\tau)$ at any time τ.

VI. RESULTS AND DISCUSSIONS

The purpose of this paper is to study various bulk properties of the gluon minijet plasma. In particular, we discuss the time evolution of the number density, the energy density, the temperature, as well as the collision-relaxation time and the transport cross section. Calculations of signatures from this equilibrating minijet plasma will be presented elsewhere.

We compare the time evolution of the energy density with that obtained in the free streaming limit (no collisions and initial rapidity distribution $\mathrm{d}N/\mathrm{d}y \propto \delta(y-\eta)$) and in the

equilibrium limit (isotropic momentum distribution in the comoving frame, at all times), i.e. the hydrodynamical evolution. For purely longitudinal expansion the energy density in the free streaming limit behaves as

$$\epsilon(\tau) = \epsilon_i \left(\frac{\tau}{\tau_{fs}}\right)^{-1} \tag{27}$$

where ϵ_i is the energy density of the gluon-minijet plasma at the time τ_{fs} where free streaming sets in.

In the equilibrium limit we have

$$n(\tau) = n_0 \left(\frac{\tau}{\tau_{eq}}\right)^{-1}, \tag{28}$$

$$\epsilon(\tau) = \epsilon_0 \left(\frac{\tau}{\tau_{eq}}\right)^{-\frac{4}{3}}, \tag{29}$$

$$T(\tau) = T_0 \left(\frac{\tau}{\tau_{eq}}\right)^{-\frac{1}{3}}. \tag{30}$$

In the above equations ϵ_0, n_0 and T_0 are the energy density, number density and temperature of the gluon plasma at $\tau = \tau_{eq}$, where equilibrium is reached. The latter two equations actually depend on the equation of state of the minijet plasma; we have assumed an ideal gas of gluons.

The evolution of the energy densities at RHIC and LHC are shown in Fig. 1 and Fig. 2 respectively. The solid lines depict the result from our self-consistent transport calculations. The dashed lines correspond to the free streaming evolution (see Eq. (27)) with the minijet initial conditions at $\tau_{fs} = \tau_0 = 1/p_0$. The dot dashed lines correspond to the $1\bigoplus 1$ hydrodynamical evolution of the energy densities (see Eq. (29)) with the same initial conditions of the minijet plasma at $\tau_{eq} = \tau_0$. The latter case represents the evolution of the energy densities assuming equilibration at $\tau = \tau_0$. It can be seen that our results lie between the free streaming and hydrodynamic limits. To see when equilibration sets in we fit our results with $\epsilon(\tau) \propto \tau^{-\alpha}$, at different times. We present our fitted values of α in Table-II and Table-III for RHIC and LHC respectively. It can be observed that as time progresses the scaling exponent α increases. This is due to the fact that at later times the collision rate among the plasma constituents increases, driving the system towards equilibrium. As a cross-check we also examine the behavior of the temperatures and number densities.

The time evolutions of the "temperatures" of the minijet plasma at RHIC and LHC are depicted in Fig. 3. It can be observed that the plasma is found to be much hotter at LHC than at RHIC. To study equilibration we have fitted our results with $T(\tau) \propto \tau^{-\alpha}$, at different times. The fitted values of α are given in Table-II and Table-III for RHIC and LHC respectively. Again we see that as time progresses the scaling exponent α increases. As already mentioned above, T should not be interpreted as a temperature in the thermodynamic sense for $\tau < \tau_{eq}$. This is because the energy-momentum tensor at those early times deviates from the ideal fluid form, which is why Eqs. (28-30) do not hold. Nevertheless, $T(\tau)$ can be taken as an indication for the time evolution of the average energy per particle even at $\tau < \tau_{eq}$.

The evolutions of the number densities are shown in Fig. 4. Not surprisingly, the plasma is found to be much denser at LHC than at RHIC. Again, we have fitted our results to

$n(\tau) \propto \tau^{-\alpha}$, at various times. The fitted values of α can be found in Table-II and Table-III for RHIC and LHC respectively. As already mentioned above, the density $n(\tau)$ decreases less fast than $\propto 1/\tau$.

The scaling exponents given in Table-II and Table-III represent the fitted values of our results ($\epsilon(\tau)$, T(τ), n(τ)) with the functional form $\tau^{-\alpha}$, at different times. For an equilibrated $1 \bigoplus 1$ dimensionally expanding plasma the scaling exponents are 4/3 for $\epsilon(\tau)$, 1/3 for T(τ) and 1 for n(τ) respectively. It can be seen from Table-II and Table-III that our scaling exponents approach those values at later times. The reader may judge himself when the system is close to equilibrium. Our choice is $\tau_{eq} \sim 4 - 5$ fm.

The time evolutions of the transport cross sections at RHIC and LHC are shown in Fig. 5. In our calculation the minijet scale p_0 evolves with collision energy, (1.13 and 2.13 GeV at RHIC and LHC, respectively; see section II). Therefore, more energetic partons are produced at LHC and the transport cross section is much smaller. These transport cross sections play a crucial role in the equilibration of the plasma, cf. Eq. (16). Since the screening mass and the momentum scale in the running coupling constant decrease with time the transport cross section, in turn, increases strongly. Therefore, despite the decreasing number density the relaxation time decreases at later time. In Fig. 6 we have displayed the time evolution of the relaxation time $\tau_c(\tau)$. One observes that the relaxation times at RHIC and LHC do not differ by much, despite the much higher density of partons obtained at LHC.

Finally, in Fig. 7 we present the time evolution of the coupling constant. One observes that the coupling seems to be weak at LHC but becomes stronger at RHIC, see also ref. [18]. One may have to include also higher order processes in the study of equilibration of the minijet plasma at RHIC, which will yield faster equilibration as compared to the present results.

VII. SUMMARY AND CONCLUSIONS

We have studied the production and equilibration of the gluon minijet plasma produced in the central region of high-energy nuclear collisions by solving the relativistic Boltzmann transport equation. The initial conditions are obtained from pQCD. We have solved the transport equation employing a collision term based on $2 \rightarrow 2$ elastic collisions. The collinear divergence in the perturbative cross section to lowest order is removed by incorporating the screening of very soft interactions by the medium. The screening mass is calculated from the non-equilibrium distribution function of the partons.

Parton equilibration in high-energy collisions has previously been discussed within the Boltzmann equation in refs. [19–21]. However, ref. [19] made an *Ansatz* for the time-dependence of the relaxation rate, $\tau_c(\tau) = \theta_0(\tau/\tau_0)^{\beta}$. It has been found that the results depend rather sensitively on the exponent β. In [20] an attempt was made to obtain an analytical expression for $\tau_c(\tau)$. However, the authors actually use equilibrium distribution functions (apart from other approximations) to derive the relaxation time, which is written as a function of temperature.

In the present work we attempted to reduce such uncertainties by coupling $\tau_c(\tau)$ to the evolution of the medium itself, leading to self-consistent dynamics. Moreover, $\tau_c(\tau)$ is determined from the medium by using the number density and transport cross section which are computed by using the actual non-equilibrium distribution functions. The treatment of

a non-equilibrium medium determining the relaxation time in an explicit and numerically computable way is one of the main contributions of our paper.

Another major difference to previous treatments lies in the choice of the initial time and initial conditions. In particular, we have taken into account that according to recent arguments regarding parton saturation the minijet scale increases with collision energy, which has a significant effect on the initial conditions. In [19–21], for example, the initial conditions were taken from the HIJING model [22] at rather late time where it is assumed that momentum isotropy is reached (in HIJING the minijet scale p_0 is assumed to be energy independent). The initial conditions used in the above studies are obtained at τ_0'= 0.7 fm at RHIC and 0.5 fm at LHC. The energy densities at these times are 3.2 GeV/fm^3 at RHIC and 40 GeV/fm^3 at LHC. We solve the transport equation starting at $\tau_0 = 1/p_0 < \tau_0'$ fm, and do not find isotropic momentum distributions at τ_0'. As our initial conditions at $\tau_0 = 1/p_0$ are rather different from those employed in [19–21], our findings regarding equilibration time and other bulk properties of the plasma differ considerably from those of the above studies.

In our study all the quantities such as $\alpha_s(\tau)$, $m_t(\tau)$, $\hat{s}(\tau)$, $n(\tau)$, $\epsilon(\tau)$ are obtained by using the non-equilibrium distribution functions. These time dependent quantities are used in a self-consistent manner to determine the evolution of the plasma. We have attempted to study equilibration without approximations which are valid only in equilibrium, and have tried to define most of the quantities in non-equilibrium. For example, we do not include a magnetic screening mass in our study because we do not find a closed expression for the magnetic screening mass in terms of the non-equilibrium distribution function in the literature. Most of the analysis of magnetic screening mass is done in thermal QCD and such calculations can not be applied to the initial non-equilibrium stage of high-energy collisions. From this point of view we are presently unable to account for magnetic screening in our non-equilibrium study. Also, the extensive numerical computations (we solve for the actual phase-space distribution function, not only for it's first moment) were presently restricted to a momentum independent relaxation time; that is, we considered the static (infinite wavelength) limit of the polarization tensor only.

In the present discussion of thermal equilibration we have restricted ourselves to $gg \to gg$ secondary elastic collisions. We hope to include $gg \to ggg$ (and vice versa) inelastic collisions in the future, which is necessary to address chemical equilibration. Our present results are based on $gg \to gg$ perturbative elastic collisons of the produced minijets at RHIC and LHC.

The present study confirms that the plasma is much denser and hotter at LHC energy. For central collisions of heavy ions at RHIC and LHC energy the minijet plasma appears close to equilibrium at a time $\tau_{eq} \simeq 4 - 5$ fm, with a temperature of 220 MeV and 380 MeV respectively. We do not obtain significantly different kinetic equilibration times of the gluon-minijet plasma at RHIC and LHC because the product of comoving parton density and transport cross-section, i.e. the kinetic equilibration rate, is similar. However, there are differences in other physical quantities such as number density, energy density and temperature. Our results indicate somewhat larger equilibration times than those obtained in the parton cascade model [23] (with fixed minijet scale p_0 and medium independent cutoff for rescattering) and HIJING [22].

For simplicity, we have not incorporated any coherent field in the present study. Including a coherent field in the initial condition may decrease the equilibration times and increase the energy density, the number density and the temperature of the plasma. We attempt to

study the production and equilibration of a QGP at RHIC and LHC with both coherent field and incoherent partons taken into account in a forthcoming paper.

ACKNOWLEDGMENTS

We thank K. Kajantie for pointing out an error in the earlier version of the paper. This manuscript has been authored under contract No. DE-AC02-98CH10886 with the U.S. Department of Energy. G.C.N. acknowledges support by the Alexander von Humboldt Foundation. A.D. is supported from the DOE Research Grant Contract No. De-FG-02-93ER-40764.

REFERENCES

[1] Proceedings of 14th Intern. Conference on Ultrarelativistic Nucleus-Nucleus Collisions (Quark Matter 99), Torino, Italy, 10-15 May 1999, Nucl. Phys. **A661**, 1c (1999).

[2] G.C. Nayak, JHEP 9802 (1998) 005, and Phys. Lett. B 442 (1998) 427; C. Spieles et al., Phys. Rev. C60 (1999) 054901.

[3] L. McLerran and R. Venugopalan, Phys. Rev. D 49 (1994) 2233 and 3352; W. Poeschl and B. Müller, Phys. Rev. D60 (1999) 114505.

[4] Yu. Kovchegov and A.H. Mueller, Nucl. Phys. B529 (1998) 451; A.H. Mueller, hep-ph/9906322.

[5] A. Kovner, L. McLerran and H. Weigert, Phys. Rev. D52 (1998) 3809 and 6231; A. Krasnitz and R. Venugopalan, Nucl. Phys. B557 (1999) 237; Y.V. Kovchegov, E. Levin and L. McLerran, hep-ph/9912367.

[6] X. Wang and M. Gyulassy, Phys. Rev. D44 (1991) 3501; K. Geiger, Phys. Rev. D46 (1992) 4965 and 4986; K.J. Eskola and K. Kajantie, Z. Phys. C75 (1997) 515; N. Hammon, H. Stöcker, and W. Greiner, Phys. Rev. C61 (1999) 014901; A. Krasnitz and R. Venugopalan, hep-ph/9909203; V. Emel'yanov, A. Khodinov, S. R. Klein and R. Vogt, Phys. Rev. C61, 044904 (2000).

[7] J.P. Blaizot and A.H. Mueller, Nucl. Phys. B289, 847 (1987); K.J. Eskola, K. Kajantie, and J. Lindfors, Nucl. Phys. B323, 37 (1989); G. Calucci and D. Treleani, Phys. Rev. D41, 3367 (1990); K.J. Eskola and M. Gyulassy, Phys. Rev. C47, 2329 (1993).

[8] K.J. Eskola, V.J. Kolhinen and P.V. Ruuskanen, Nucl. Phys. B535 (1998) 351; K.J. Eskola, V.J. Kolhinen and C.A. Salgado, Euro. Phys. J. C9 (1999) 61.

[9] M. Glueck, E. Reya and A. Vogt, Euro. Phys. J. C5 (1998) 461.

[10] K. J. Eskola, K. Kajantie, P. V. Ruuskanen and K. Tuominen, Nucl. Phys. B570 (2000) 379.

[11] T.S. Biro, Int. J. Mod. Phys. E1 (1992) 39; T.S. Biro, B. Müller, and X. Wang, Phys. Lett. B283 (1992) 171

[12] J.D. Bjorken, Phys. Rev. D27 (1983) 140.

[13] T.S. Biro, E. van Doorn, B. Müller, M.H. Thoma and X.N. Wang, Phys. Rev. C48 (1993) 1275

[14] G. Baym, Phys. Lett. B 138 (1984) 18; K. Kajantie and T. Matsui, Phys. Lett. B 164 (1985) 373; G. Baym, H. Monien, C.J. Pethick and D.G. Ravenhall, Nucl. Phys. A 525 (1991) 415c.

[15] A. Hosoya and K. Kajantie, Nucl. Phys. B250 (1985) 666.

[16] P. Danielewicz and M. Gyulassy, Phys. Rev. D31 (1985) 53.

[17] M. Gyulassy, Y. Pang, and B. Zhang, Nucl. Phys. A626 (1997) 999; B. Zhang, Comput. Phys. Commun. 109 (1998) 193.

[18] S. A. Bass and B. Müller, Phys. Lett. B471 (1999) 108.

[19] H. Heiselberg and X.N. Wang, Phys. Rev. C53 (1996) 1892.

[20] H. Heiselberg and X.N. Wang, Nucl. Phys. B462 (1996) 389.

[21] S.H. Wong, Nucl. Phys. A607 (1996) 442.

[22] X.N. Wang, Phys. Rep. 280 (1997) 287.

[23] K. Geiger, Phys. Rep. 258 (1995) 237.

Figure captions

FIG. 1. Time evolution of the energy density of the gluon-minijets at RHIC. The solid line is obtained from the self-consistent solution of the transport equation. The dashed line correspond to the free streaming and hydrodynamic limits with the same initial minijet conditions at $\tau_0 = 1/p_0$.

FIG. 2. Time evolution of the energy density of the gluon-minijets at LHC. The solid line is obtained from the self-consistent solution of the transport equation. The dashed line correspond to the free streaming and hydrodynamic limits with the same initial minijet conditions at $\tau_0 = 1/p_0$.

FIG. 3. Time evolution of the temperatures of the gluon-minijets at RHIC and LHC.

FIG. 4. Time evolution of the number densities of the gluon-minijets at RHIC and LHC.

FIG. 5. Time evolution of the in-medium transport cross sections for the $gg \to gg$ process at RHIC and LHC.

FIG. 6. Time evolution of the kinetic relaxation time $\tau_c(\tau)$ at RHIC and LHC.

FIG. 7. Time evolution of the strong coupling constant $\alpha_s(\tau)$ at RHIC and LHC.

	$\sqrt{s}$ (GeV)	p_0 (GeV)	A-B	n_0 (fm^{-3})	ϵ_0 (GeV/fm^3)	T_0 (GeV)
RHIC	200	1.13	Au-Au	34.3	56	0.535
LHC	5500	2.13	Pb-Pb	321.6	1110	1.13

TABLE I. Initial conditions for the pre-equilibrium evolution of the plasma, as obtained from the number and energy of gluon-minijets with $p_t > p_0$.

RHIC	τ (fm)	α (for $\epsilon(\tau)$)	α (for T(τ))	α (for n(τ))
	0.5	1.13	0.286	0.80
	1.0	1.15	0.290	0.76
	1.5	1.17	0.295	0.75
	2.0	1.2	0.302	0.76
	2.5	1.22	0.305	0.77
	3.0	1.23	0.31	0.782
	3.5	1.25	0.312	0.8
	4.0	1.26	0.315	0.83
	4.5	1.27	0.32	0.85

TABLE II. Exponents α obtained by fitting our results with the functional form $\tau^{-\alpha}$ at RHIC.

LHC	τ (fm)	α (for $\epsilon(\tau)$)	α (for T(τ))	α (for n(τ))
	0.5	1.118	0.29	0.774
	1.0	1.164	0.297	0.75
	1.5	1.185	0.302	0.751
	2.0	1.21	0.306	0.77
	2.5	1.227	0.308	0.8
	3.0	1.240	0.31	0.825
	3.5	1.251	0.314	0.85
	4.0	1.262	0.317	0.875
	4.5	1.271	0.318	0.897
	5.0	1.28	0.32	0.92
	5.5	1.28	0.32	0.92
	6.0	1.28	0.32	0.93

TABLE III. Exponents α obtained by fitting our results with the functional form $\tau^{-\alpha}$ at LHC.

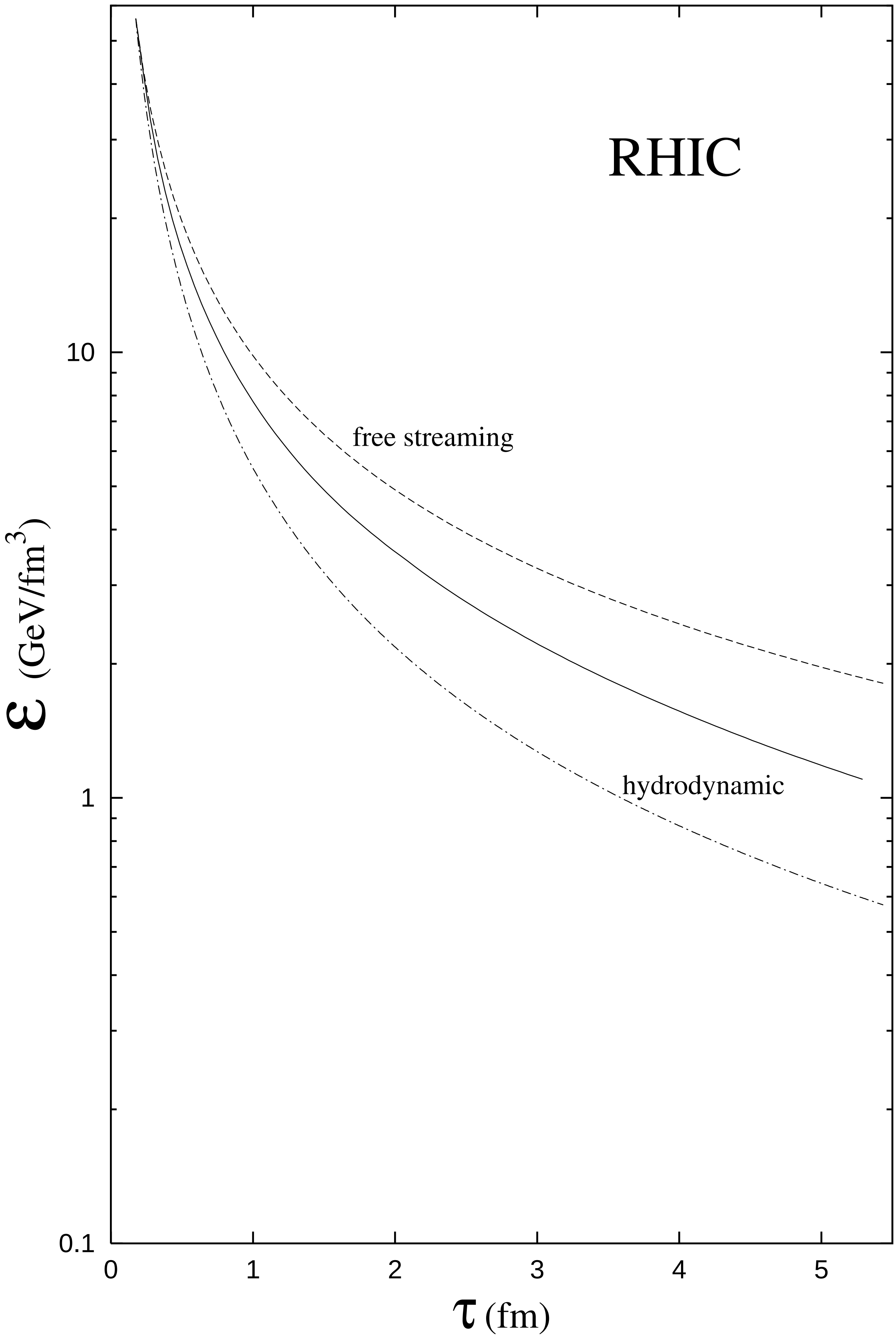
RHIC
free streaming
hydrodynamic
10
1
0.1
0
1
2
3
4
5
ε (GeV/fm^3)
τ (fm)

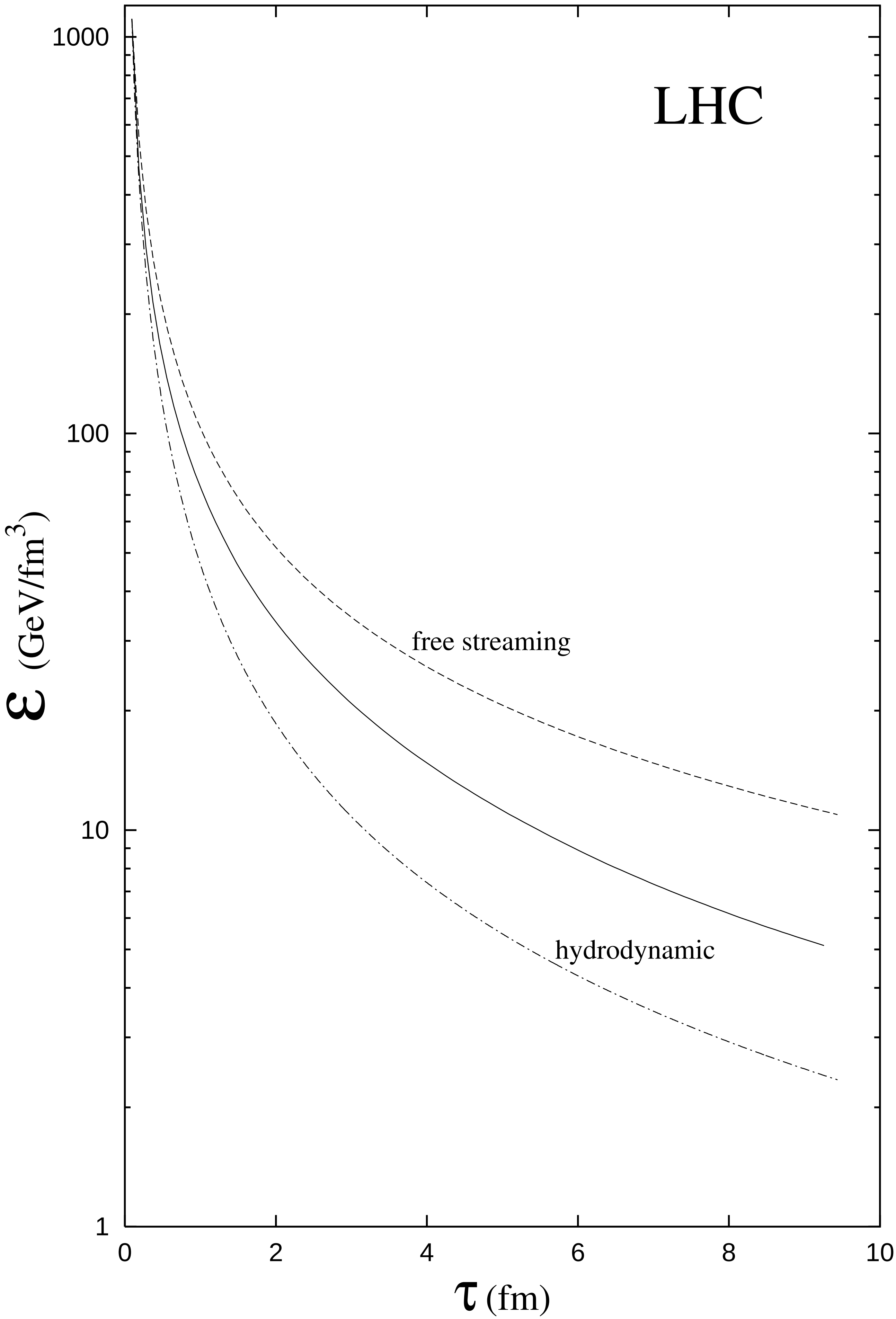

LHC
free streaming
hydrodynamic
1000
100
10
1
0
2
4
6
8
10
ε (GeV/fm³)
τ (fm)

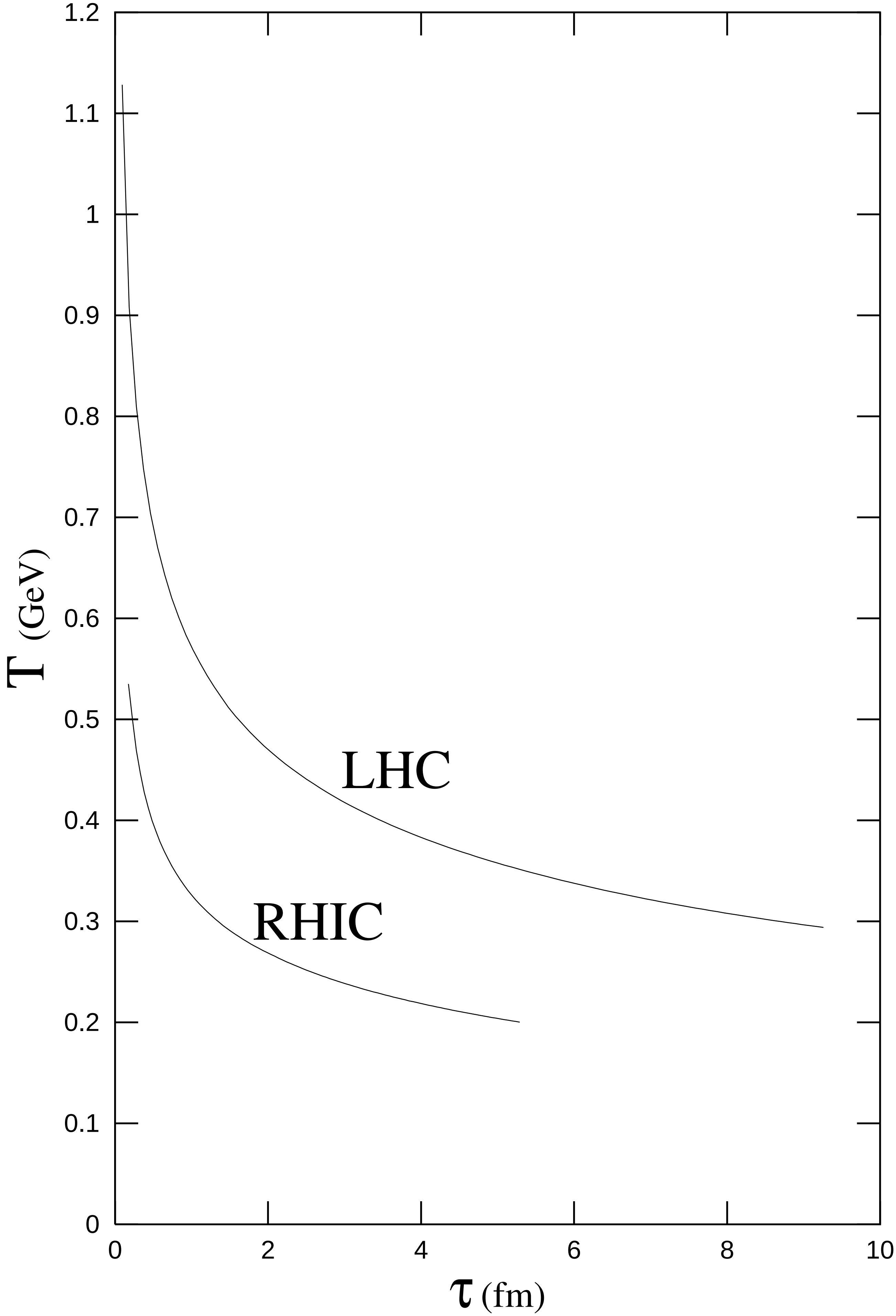

1.2
1.1
1
0.9
0.8
0.7
0.6
0.5
0.4
0.3
0.2
0.1
0
T (GeV)
LHC
RHIC
0
2
4
6
8
10
τ (fm)

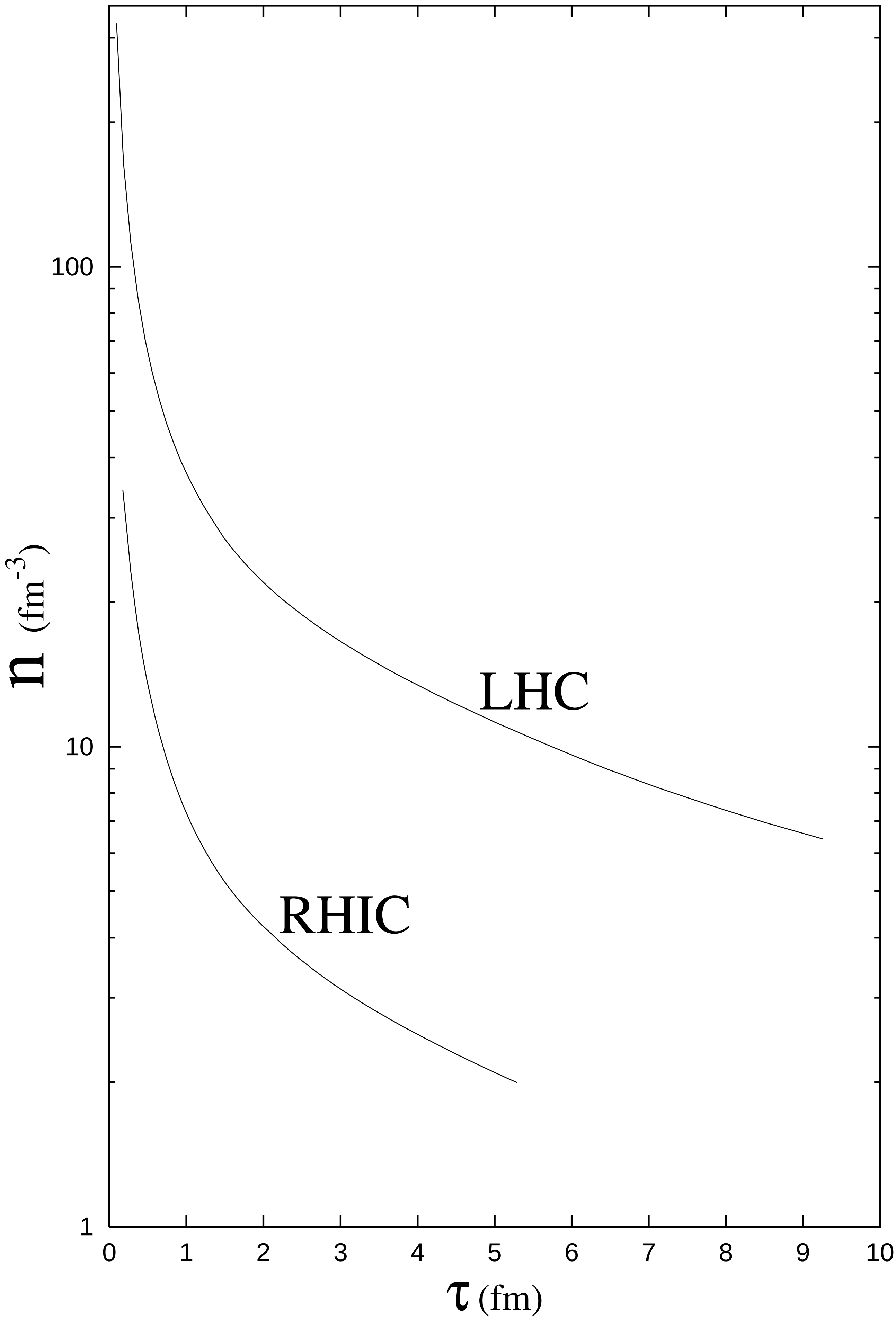

n (fm-3)
100
10
1
LHC
RHIC
0
1
2
3
4
5
6
7
8
9
10
τ (fm)

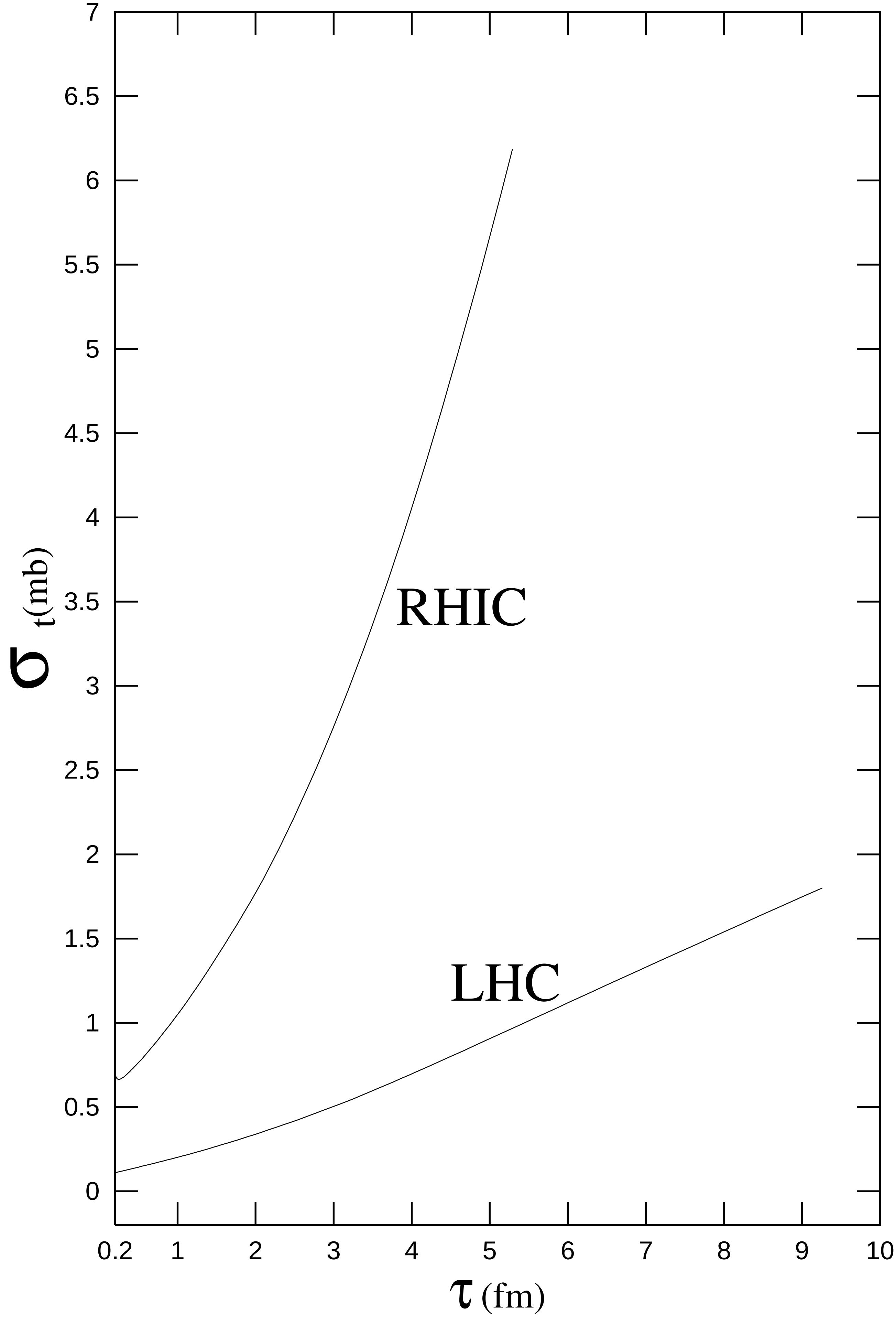

RHIC
LHC
σ_t(mb)
τ (fm)
0
0.5
1
1.5
2
2.5
3
3.5
4
4.5
5
5.5
6
6.5
7
0.2
1
2
3
4
5
6
7
8
9
10

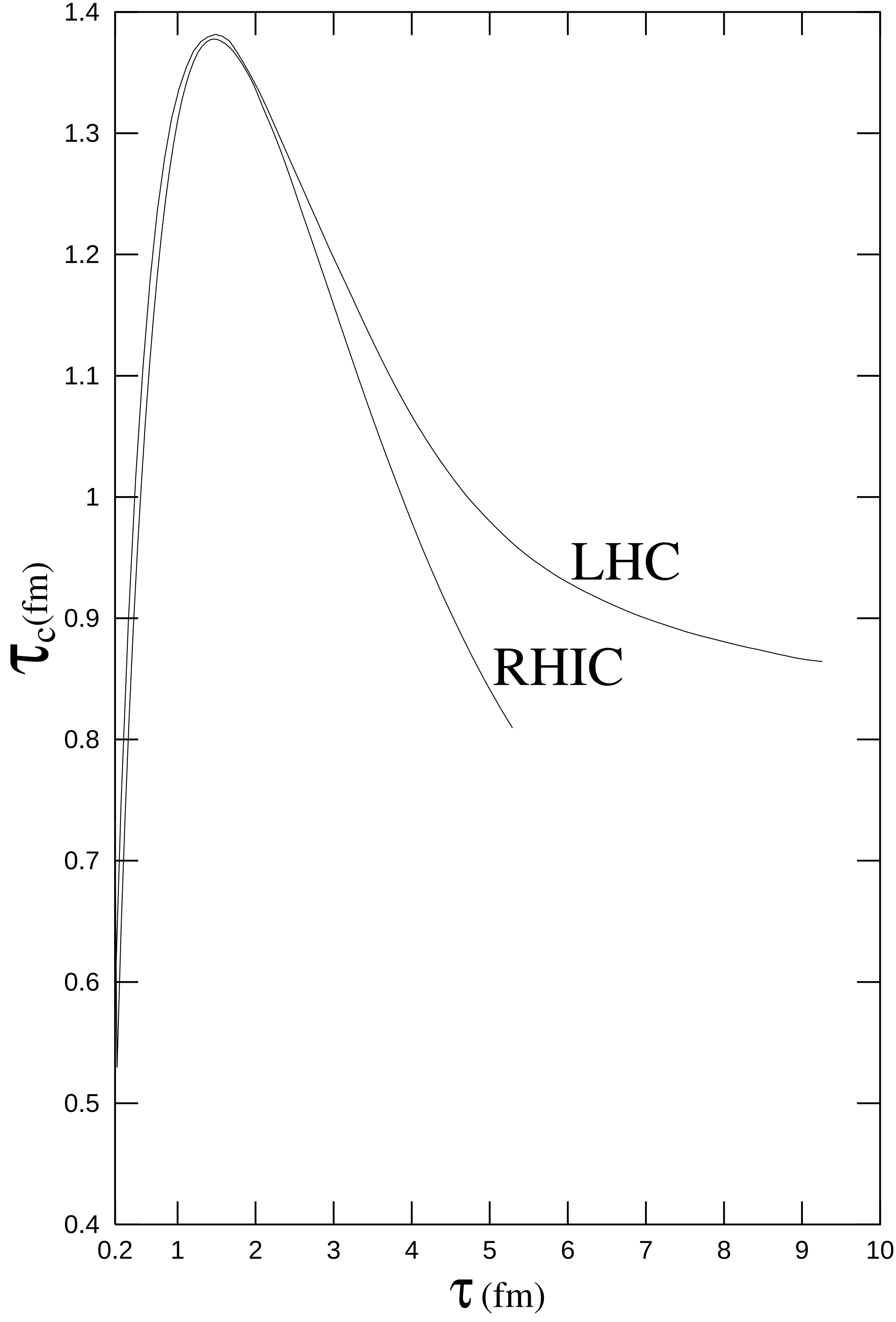

1.4
1.3
1.2
1.1
1
0.9
0.8
0.7
0.6
0.5
0.4
0.2
1
2
3
4
5
6
7
8
9
10
LHC
RHIC
τc(fm)
τ (fm)

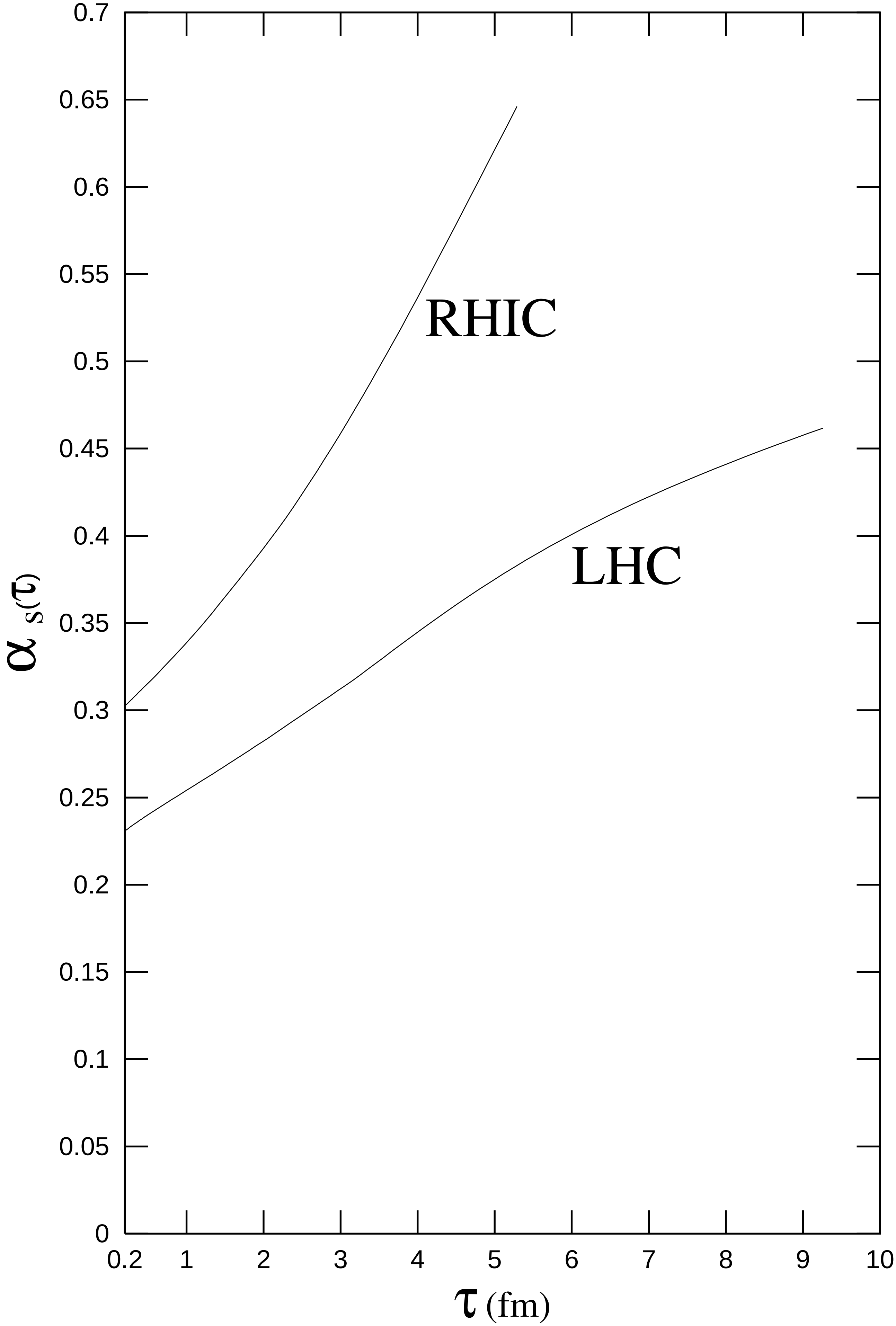

0.7
0.65
0.6
0.55
0.5
0.45
0.4
0.35
0.3
0.25
0.2
0.15
0.1
0.05
0
0.2
1
2
3
4
5
6
7
8
9
10
RHIC
LHC
$\alpha_S(\tau)$
τ (fm)